Optics Letters

Sum-frequency generation in lithium-niobate-on-insulator microdisk via modal phase matching

Xiaona Ye,[1] Shijie Liu,[1] Yuping Chen,[1] Yuanlin Zheng,[1,3] and Xianfeng Chen[1,2,4]

[1]State Key Laboratory of Advanced Optical Communication Systems and Networks, School of Physics and Astronomy, Shanghai Jiao Tong University, Shanghai 200240, China
[2]Collaborative Innovation Center of Light Manipulations and Applications, Shandong Normal University, Jinan 250358, China
[3]e-mail: ylzheng@sjtu.edu.cn
[4]e-mail: xfchen@sjtu.edu.cn

Received 15 November 2019; revised 11 December 2019; accepted 12 December 2019; posted 16 December 2019 (Doc. ID 383450); published 10 January 2020

Whispering-gallery-mode microresonators, one of the most important components of photonic integrated circuits, have the ability to dramatically boost light–matter interactions. In this Letter, we demonstrate effective sum-frequency generation via modal phase matching in a triply resonant lithium-niobate-on-insulator microdisk resonator through two individual continuous wave pumps working in the communication band. The sum-frequency conversion efficiency is measured to be 2.22×10^{-6} mW^{-1}. This work shows a high-efficiency frequency convertor that may be applied in on-chip integrated optics in the future.

https://doi.org/10.1364/OL.383450

Single-crystal lithium niobate ($LiNbO_3$, LN) has rich and outstanding physical properties, such as a broad transmission window (0.4–5.0 μm), large second-order susceptibility, relatively high refractive indices, large piezoelectricity, and so on [1]. In terms of optical information processing, optical components are gradually replacing electrical components because of their large operating bandwidth, wavelength division multiplexing, and no electromagnetic crosstalk. LN has shown significant potential as a versatile platform for manipulating photons due to its excellent characteristics. The integrated optical chips based on LN platform are gradually coming into practice [2].

Whispering-gallery-mode (WGM) microresonators, one of the most important components of the photonic chip, offer the capability to trap photons in a small volume by total internal reflection for a long duration. The strong cavity resonance and long photon lifetimes lead to the generation of strong electric fields and effectively enhance the interaction between light and matter [3]. During the past few decades, the research on WGM microresonators has increasingly thrived worldwide to enable applications ranging from optical signal processing [4], optical sensing [5], tunable optical filters [6], low threshold lasing [7], and nonlinear optics [8–10] to quantum electrodynamics [11] and cavity optomechanics [12,13]. Because of its high second-order nonlinear effect, LN has great advantages in nonlinear fields compared with other materials, and various nonlinear optical effects have been demonstrated in bulk LN WGM resonators in previous research, such as sum-frequency generation (SFG) [14]. However, these millimeter-scale WGM resonators fabricated by mechanical cutting and polishing techniques [15] are bulky and not conducive to integration. Recently, thin-film lithium niobate on insulator (LNOI) has become commercially available, which has sparked significant interest in the platform for photonic integrated circuits (PICs). Benefiting from the maturity of various LNOI micro-fabrication techniques, the quality (Q)-factor of LNOI microresonator has reached the order of 10^7 in recent years [16]. The strong nonlinear optical effects, including second-harmonic generation (SHG), third-harmonic generation [17], effective four-wave mixing [18], spontaneous parametric down conversion [19], optical comb generation [20], and electro-optic [21], thermo-optic [22,23], and optomechanical effects [24], have been observed in such high-Q WGM microresonators on the LNOI platform.

Among these, SFG can effectively convert low-frequency weak light down to one single photon to high-frequency optical signal with the aid of a strong pump [25]. The infrared, far-infrared, and even sub-THz photons [26,27] can also be efficiently converted to visible light through the SFG process and detected by commercially available visible detectors with low noise. Besides, efficient manipulation of the frequency and the pulse shape of single-photon signals [28] for interfacing optical flying qubits with narrowband atomic quantum memories [29] have also been demonstrated by using the SFG process, because it does not disturb the quantum state [30]. Therefore, it is rather important to realize the SFG process in WGM resonators to expand its application in PICs. Although the implementation of SFG has been reported in LN microdisk resonators [25], it is still difficult to observe SFG in the microdisk by using two continuous-wave (cw) pumps due to the difficulty of the dispersion control and the relative low mode density. Ideally, the two pump lasers and the SFG signal at different frequencies should

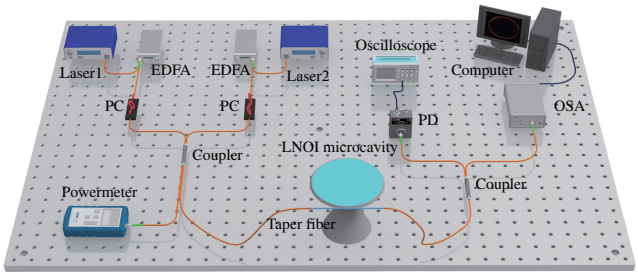

Fig. 1. Schematic illustration of the experimental setup. EDFA, erbium-doped fiber amplifier; PC, polarization controller; Coupler, 2 × 2 port fiber coupler; PD, InGaAs avalanche photodetector; OSA, optical spectrum analyzer.

be simultaneously triply resonant in such microresonators to reach the high-efficiency-frequency conversion, which brings more difficulties to design the microresonators and to carry out the experiment.

In this Letter, we report the experimental observation of an effective SFG process via modal phase matching in a triply resonant LNOI microdisk resonator with strongly nondegenerate frequencies. The efficient SFG is observed through two individual cw pumps with several-milliwatt input power, working in the communication band. In our experiment, the conversion efficiency is measured to be about 2.22×10^{-6} mW^{-1}, which is one order of magnitude higher than in previous report [25]. We have demonstrated that the intensity of the SFG signal is linearly proportional to the pump power of one laser. The relationship between the SFG power and the wavelength of one pump laser is investigated while fixing the wavelength of the other. Besides, we also analyze the SFG process when the pumps are, respectively, tuned to two adjacent WGMs and high-order modes.

Our experimental setup is schematically depicted in Fig. 1. Pump 1 and Pump 2 are launched from two external cavity tunable lasers (Laser 1 and Laser 2) in the telecommunication C band and individually amplified by an erbium-doped fiber amplifier (EDFA) (amplification is not necessary if laser sources have enough power). The polarizations of pump signals are controlled by polarization controllers (PC). The two lasers are combined by a 2 × 2 50 : 50 single-mode fiber coupler and launched into a tapered fiber on one path. At the same time, the input power is monitored by a powermeter on the other path. In our experiment, the tapered fiber with a waist diameter of ∼ 1 μm is made by using a single-mode telecom fiber through the heating-and-pulling method. The LNOI microdisk sample is mounted on a precise 3D nanostage for precise positioning. The tapered fiber couples light into and out of the microdisk through the evanescent wave. The transmitted light coupled out from the taper fiber-microdisk coupling system is sent to another 1 × 2 90 : 10 fiber coupler. The signal from the 90% port is received by an optical spectrum analyzer (OSA). An InGaAs photodetector (PD) and an oscilloscope are used to simultaneously measure the quality factors of the resonator and monitor the coupling between the tapered fiber and microdisk from the 10% port of the fiber coupler. The LNOI microdisk is also monitored by an optical microscope from a top view for both coupling optimization and the observation of the SFG process.

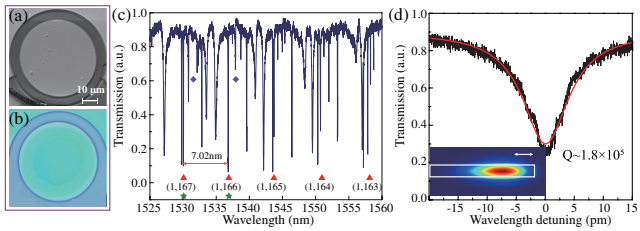

Fig. 2. (a) Top-view scanning electron microscope (SEM) image of the LNOI microdisk after FIB processing. (b) Optical microscope image of the microdisk after hydrofluoric acid etching. The diameter of the microdisk is 49 μm. (c) Normalized transmission spectrum of the LNOI microdisk at telecommunication wavelengths. The corresponding mode orders are marked, and the FSR of the microdisk is 7.02 nm. (d) The Lorentz fitting (red curve) reveals a Q factor of 1.8×10^5. Inset: the finite element mode simulation of fundamental TE mode at 1536.88 nm.

In our experiment, the microdisk resonator is fabricated on commercial LNOI nanofilms (NANOLN, Jinan Jingzheng Electronics Co., Ltd.). A layer of Z-cut single crystalline LN thin film with a thickness of 300 nm is bonded on the top of a 2-μm-thick silica layer, and the bottom layer is a 0.5-mm-thick LN substrate. The LNOI microdisk is fabricated at the Center for Advanced Electronic Materials and Devices of Shanghai Jiao Tong University. The fabrication consists of two steps: (1) focus ion beam (FIB) etching of the thin-film sample to directly write the microdisk, and (2) chemical wet etching of the fabricated sample in a solution of 5% hydrofluoric acid diluted with water to form the freestanding LN microdisk on silica pedestal by selectively removing the silica layer under the LN thin film. The diameter of our fabricated LNOI microdisk is 49 μm. The topography of the microdisk sample after FIB processing is analyzed by scanning electronic microscopy, as shown in Fig. 2(a). It is clear that our microdisk has an ultrahigh smooth surface, which can achieve sub-nanometer rms precision. Figure 2(b) exhibits an optical microscope image of our microdisk after hydrofluoric acid etching.

The transmission spectrum characterizing the optical modes of the microcavity is measured through a taper fiber coupling system. To avoid thermal broadening and nonlinear effects, Laser 1 with a very low input power (< 100 μW) is used to scan the transmission spectrum over a wide wavelength range from 1525 nm to 1560 nm, as shown in Fig. 2(c). According to the adjacent WGMs, the measured free spectral range (FSR) of the modes is 7.02 nm, which is consistent with the simulation result 7.03 nm. Typical resonance wavelengths labeled with a red triangle of the first radial orders of TE modes have been determined by comparison with a finite-element simulation. The corresponding mode order of observed WGM can be identified by numerical simulation and then marked accordingly in the transmission spectrum. The indices (q, m) denote radial and azimuthal mode numbers, respectively. We should point out that transverse magnetic (TM)-like modes in the telecommunication wavelength range are not supported by our microdisk according to the simulation results, since the thickness of our LN film is only 300 nm. An accurate measurement of the Q factor is performed by fine scanning without thermal broadening. As illustrated in Fig. 2(d), the high Q-factor of a mode around 1536.88 nm is estimated to be 1.8×10^5 by Lorentz fitting (red solid line), in which the full width at half-maximum

is 8.5 pm. The mode at 1536.88 nm is identified as TE(1, 166). It corresponds to the first transverse electric mode, which has the largest effective refractive index and is used to excite harmonic modes at higher spatial orders. Accurate measurement of the Q factor in the visible range is not performed due to the lack of a tunable laser source. However, the Q factor can be expected to be equivalent to that in C band [31]. The inset in Fig. 2(d) presents the simulation result of cross-sectional mode profile at 1536.88 nm. From the mode distribution, we can see that the resonance corresponding to the TE-like mode is well confined in the microdisk.

First, Pump 1 at 5 mW is incident to the LNOI microdisk while slowly scanning the wavelength. An efficient SHG via modal phase matching is observed when the Pump 1 wavelength is tuned into the resonance of the TE(1, 166) mode at 1536.88 nm. Then, by adjusting the wavelength of Pump 1, the SHG signal is observed when tuned into the central wavelength of 1529.76 nm corresponding to the WGM of TE(1,167), as marked with a red triangle in Fig. 2(c). Next, the wavelength of Pump 1 is locked at 1529.76 nm without changing the pump power (5 mW), and we add Pump 2 from tunable Laser 2 into the microdisk. When adjusting the wavelength of Pump 2 around 1543.78 nm corresponding to the TE(1, 165) mode as marked in Fig. 2(c), two peaks of the SHG signal occur at the wavelengths 764.88 nm and 771.89 nm, and the SFG peak at the wavelength 768.37 nm can also be observed at the same time, as shown in Fig. 3(a). It is clear that the intensity of the SFG signal is much higher than the SHG signal. The intensities of nonlinear optical signals depend on the spatial overlap of the involved WGMs and the frequency overlap of the pumps (Pump 1 and Pump 2) and the SFG signal with the resonances of the resonator [25]. In our experiments, the phase-matching condition occurs between the TE(1, 166) mode and higher-order SHG modes [31]. The SHG of TE(1, 167) and TE(1, 165) does not satisfy the phase-matching condition, which decreases the nonlinear conversion efficiency. In contrast, the two modes of TE(1, 167) and TE(1, 165) possess wave vector mismatches of $+\Delta k$ and $-\Delta k$ with respect to TE(1, 166). The phase-matching condition can be satisfied through counteracting such phase mismatch when the pumps are excited from TE(1, 167) and TE(1, 165) modes. Therefore, such an SFG signal generated through this method satisfies the modal-phase-matching condition and generates a much stronger signal than their individual SHG. The inset of Fig. 3(a) shows the optical micrograph of the bright-scattered SFG wave travelling around the LNOI microdisk periphery.

Next, we fix the wavelength of Pump 1 at 1529.76 nm corresponding to the TE(1, 167) mode and tune the central wavelength of Pump 2 off the mode-phase-matching condition, which are labeled by green stars in Fig. 2(c), respectively. The SHG signals of the two pumps appear at 764.88 nm and 768.44 nm. The SFG signal can still be observed, and its wavelength is 766.65 nm, as shown in Fig. 3(b). In this case, the SHG process holds a dominant position during the competition between SHG and SFG processes, and the intensity of SFG is weaker than the SHG due to a larger phase mismatch. The image of the SHG and SFG light is shown in the inset of Fig. 3(b), which is much darker than the inset in Fig. 3(a). In the above two situations, Pump 1 and Pump 2 are both first radial order TE modes. Next, we tune two pumps to higher-order modes, which are marked in Fig. 2(c) with purple

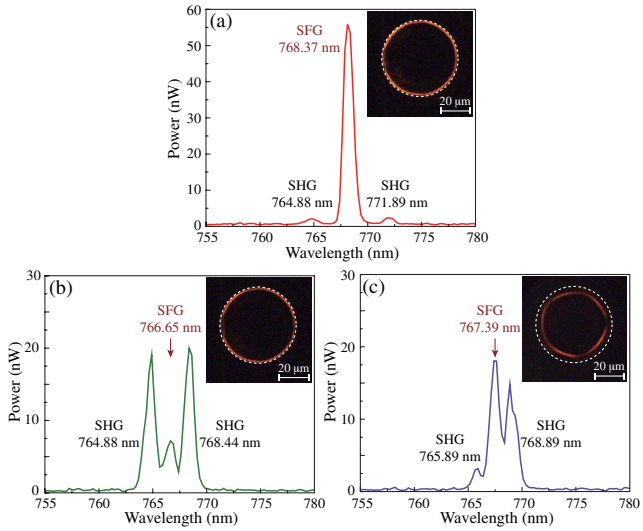

Fig. 3. Experimental results of SFG. (a) Spectrum of the generated SFG and SHG. The peak of SFG through modal phase matching is at 768.37 nm. The signals at 764.88 nm and 771.89 nm are SHG of the two pumps. Inset: top-view optical micrograph of the scattered SFG light travelling around the LNOI microdisk periphery. The white dotted circle shows the profile of the microdisk. (b) and (c) Spectra of SFG and SHG when the pumps are, respectively, tuned to two adjacent first-order WGMs and high-order modes. Insets in (b) and (c) images of SHG and SFG light scattering from the microdisk.

diamonds. Figure 3(c) shows the generated SFG signal spectra when the wavelengths of pumps are tuned to 1531.78 nm and 1537.78 nm, where the central wavelength of the SFG signal is about 767.39 nm. It can be observed from the inset of Fig. 3(c) that the higher-order mode is closer to the center of the microdisk and is slightly reduced in brightness. The periodic bright–dark changes of the mixed light of SHG and SFG can also be clearly observed. The low efficiency is caused by phase mismatching and less mode overlapping. It is worth mentioning that there is a large sum-frequency bandwidth in our work, as the wavelength of one pump laser can be tuned over a broad spectral range while fixing that of the other.

Further, we record the power of the SFG signal versus the incident power of Pump 2 and its wavelength detuning. In the case of modal phase matching, the power of Pump 1 is kept at 5 mW, and the power of Pump 2 is changed from 0 to 5 mW. As illustrated in Fig. 4(a), the observed SFG signal is linearly dependent on the incident Pump 2 power. The fitted line (red solid line) perfectly matches the measured data (blue dots) with the goodness of fit (R^2) being 0.997. The SFG conversion efficiency is defined as $P_{SFG}/(P_{P1}P_{P2})$, where P_{SFG}, P_{P1}, and P_{P2} is the power of the SFG signal, Pump 1, and Pump 2, respectively. The normalized conservation efficiency in our experiment is about 2.22×10^{-6} mW^{-1}, which is improved one order of magnitude than the one reported in Ref. [25]. Nevertheless, the tapered fiber used in our experiment is in allusion to the communication band, and the distinct difference between pumps and signal modes limits the mode matching and efficient outward coupling [32]. Therefore, the measured conversion efficiency of the SFG achieved in our microdisk is much lower than the actual value. Such a problem can be solved by further

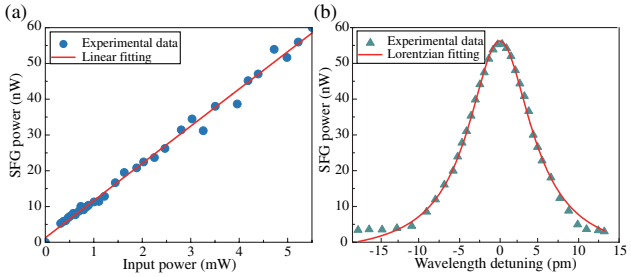

Fig. 4. (a) In the modal-phase-matching situation, the power of SFG signals changes with the incident power of the Pump 2 and its linear fitting when the intensity of Pump 1 is fixed at 5 mW. (b) SFG power versus Pump 2 wavelength detuning with the input power of 5 mW when the wavelength of Pump 1 is fixed at 1529.76 nm.

optimizing the coupling scheme of short-wavelength optical signals, such as introducing an add-drop coupling system to couple the pump and SFG signal individually. In addition, a deformed chaotic LN microcavity that features directional emission and high Q factors can be designed to realize broadband coupling [33]. The conversion efficiency can also be improved by precisely designing the geometry structure of microresonators, including radius, thickness, and periodical poling, to fulfill the quasi-phase matching scheme.

Finally, we tune the wavelength of Pump 2 with the fixed power 5 mW around the resonance mode 1543.78 nm of the LNOI microdisk and fix the wavelength of Pump 1 at 1529.76 nm. In this situation, the intensity variation of the SFG signal with the Pump 2 wavelength detuning is plotted in Fig. 4(b). The maximum SFG signal is obtained when the Pump 2 wavelength is adjusted to the resonance mode at 1543.78 nm. However, the intensity of the SFG signal gradually decreases and tends to zero when the wavelength detuning increases to the off-resonance of microdisk. The experimental data are in good agreement with the Lorentzian fitting.

In conclusion, in this Letter, we demonstrate the effective generation of sum-frequency in a triply resonant LNOI microdisk resonator. The efficient SFG is observed via a modal-phase-matching method with several-milliwatt input power of two cw pumps working in the communication band. The conversion efficiency is measured to be 2.22×10^{-6} mW^{-1}, which raises one order of magnitude at the condition of a relatively low Q factor compared with previous work. Our work shows a high-efficiency frequency convertor that may be applied in on-chip integrated optics in the future.

Funding. National Key R&D Program of China (2017YFA0303700, 2018YFA0306300); National Natural Science Foundation of China (11604206, 11734011); Foundation for Development of Science and Technology of Shanghai (17JC1400400).

Disclosures. The authors declare no conflicts of interest.

REFERENCES

1. C. Wang, M. J. Burek, Z. Lin, H. A. Atikian, V. Venkataraman, I. C. Huang, P. Stark, and M. Lončar, Opt. Express **22**, 30924 (2014).
2. Y. F. Kong, F. Bo, W. W. Wang, D. H. Zheng, H. D. Liu, G. Q. Zhang, R. Rupp, and J. J. Xu, Adv. Mater. 1806452 (2019).
3. J. Lin, Y. Xu, Z. Fang, M. Wang, J. Song, N. Wang, L. Qiao, W. Fang, and Y. Cheng, Sci. Rep. **5**, 8072 (2015).
4. M. Pöllinger and A. Rauschenbeutel, Opt. Express **18**, 17764 (2010).
5. F. Vollmer and L. Yang, Nanophotonics **1**, 267 (2012).
6. B. E. Little, S. T. Chu, H. A. Haus, J. Foresi, and J. P. Laine, J. Lightwave Technol. **15**, 998 (1997).
7. S. M. Spillane, T. J. Kippenberg, and K. J. Vahala, Nature **415**, 621 (2002).
8. J. U. Furst, D. V. Strekalov, D. Elser, M. Lassen, U. L. Andersen, C. Marquardt, and G. Leuchs, Phys. Rev. Lett. **104**, 153901 (2010).
9. G. P. Lin, A. Coillet, and Y. K. Chembo, Adv. Opt. Photon. **9**, 828 (2017).
10. X. Y. Zhang, Q. T. Cao, Z. Wang, Y. X. Liu, C. W. Qiu, L. Yang, Q. H. Gong, and Y. F. Xiao, Nat. Photonics **13**, 21 (2019).
11. T. Aoki, B. Dayan, E. Wilcut, W. P. Bowen, A. S. Parkins, T. J. Kippenberg, K. J. Vahala, and H. J. Kimble, Nature **443**, 671 (2006).
12. T. J. Kippenberg and K. J. Vahala, Science **321**, 1172 (2008).
13. C. Dong, V. Fiore, M. C. Kuzyk, and H. Wang, Science **338**, 1609 (2012).
14. D. V. Strekalov, A. S. Kowligy, Y. P. Huang, and P. Kumar, New J. Phys. **16**, 053025 (2014).
15. T. Beckmann, H. Linnenbank, H. Steigerwald, B. Sturman, D. Haertle, K. Buse, and I. Breunig, Phys. Rev. Lett. **106**, 143903 (2011).
16. R. B. Wu, J. H. Zhang, N. Yao, W. Fang, L. L. Qiao, Z. F. Chai, J. T. Lin, and Y. Cheng, Opt. Lett. **43**, 4116 (2018).
17. J. T. Lin, N. Yao, Z. Z. Hao, J. H. Zhang, W. B. Mao, M. Wang, W. Chu, R. B. Wu, Z. W. Fang, L. L. Qiao, W. Fang, F. Bo, and Y. Cheng, Phys. Rev. Lett. **122**, 173903 (2019).
18. S. J. Liu, Y. L. Zheng, Z. W. Fang, X. N. Ye, Y. Cheng, and X. F. Chen, Opt. Lett. **44**, 1456 (2019).
19. R. Luo, Y. He, H. X. Liang, M. X. Li, J. W. Ling, and Q. Lin, Phys. Rev. Appl. **11**, 034026 (2019).
20. M. Zhang, B. Buscaino, C. Wang, A. Shams-Ansari, C. Reimer, R. R. Zhu, J. M. Kahn, and M. Lončar, Nature **568**, 373 (2019).
21. C. Wang, M. Zhang, X. Chen, M. Bertrand, A. Shams-Ansari, S. Chandrasekhar, P. Winzer, and M. Lončar, Nature **562**, 101 (2018).
22. X. Sun, H. X. Liang, R. Luo, W. C. Jiang, X. C. Zhang, and Q. Lin, Opt. Express **25**, 13504 (2017).
23. J. Wang, B. W. Zhu, Z. Z. Hao, F. Bo, X. L. Wang, F. Gao, Y. G. Li, G. Q. Zhang, and J. J. Xu, Opt. Express **24**, 21869 (2016).
24. Z. W. Fang, S. Haque, J. T. Lin, R. B. Wu, J. H. Zhang, M. Wang, J. X. Zhou, M. Rafa, T. Lu, and Y. Cheng, Opt. Lett. **44**, 1214 (2019).
25. Z. Z. Hao, J. Wang, S. Ma, W. B. Mao, F. Bo, F. Gao, G. Q. Zhang, and J. J. Xu, Photon. Res. **5**, 623 (2017).
26. L. J. Ma, O. Slattery, and X. Tang, Phys. Rep. **521**, 69 (2012).
27. D. V. Strekalov, A. A. Savchenkov, A. B. Matsko, and N. Yu, Opt. Lett. **34**, 713 (2009).
28. M. G. Raymer and K. Srinivasan, Phys. Today **65**(11), 32 (2012).
29. M. S. Shahriar, P. Kumar, and P. R. Hemmer, J. Phys. B **45**, 124018 (2012).
30. P. Kumar, Opt. Lett. **15**, 1476 (1990).
31. S. J. Liu, Y. L. Zheng, and X. F. Chen, Opt. Lett. **42**, 3626 (2017).
32. Y. H. Li, X. F. Jiang, G. M. Zhao, and L. Yang, "Whispering gallery mode microresonator for nonlinear optics," arXiv:1809.04878 (2018).
33. L. Wang, C. Wang, J. Wang, F. Bo, M. Zhang, Q. H. Gong, M. Lončar, and Y. F. Xiao, Opt. Lett. **43**, 2917 (2018).